An Investigation Of Angle-of-Arrival Radar Target Simulation for Automotive Radar

Project Report

Mikkel Filt Bengtson

Aalborg University
Department of Electronic Systems
Fredrik Bajers Vej 7B
DK-9220 Aalborg Ø

AALBORG UNIVERSITY
STUDENT REPORT

Electronic Systems
Aalborg University
http://www.aau.dk

Title:
An Investigation Of Angle-of-Arrival Radar Target Simulation for Automotive Radar

Theme:
Master thesis

Project Period:
Spring Semester 2023

Project Group:
CT10 - 1020

Participant(s):
Mikkel Filt Bengtson

Supervisor(s):
Wei Fan
Fengchun Zhang

Page Numbers: 20

Date of Completion:
June 1, 2023

Abstract:

Automotive mmWave radar is becoming more accessible,, and is expected to be more widely used in autonomous driving sensor setup. integrated circuits (IC) mmWave radar allows for compact multiple inputs multiple outputs (MIMO) radar designs enabling automotive radars to have angular target estimation. Higher safety standards and increased complexity of radar setup increases the requirements for testing setup. Academia along with the industry are developing radar target simulation (RTS) systems which can handle the new test requirements. The different methodologies for simulating targets are reviewed along with methods for optimizing the simulated targets angle using fewer target emulator (TE) are reviewed. A new flexible method using a superposition of two TE for simulating angle along with a direct modulation technique is presented.
The new presented method is simulated, showing the capabilities of the method. It was possible to simulated different targets with multiple TEs, however, the technique lacks the control of the side-lobes of the angular response which might result in ghost targets. Simulation of RTS systems is performed for evaluating the two main angular simulation methods, arbitrary angle of arrival (AAOA) and flexible direction of arrival (FDOA) by comparing them to a TE placed at the wanted angle. Precise Reconstruction is possible using the FDOA, however, the method fails when considering MIMO radar system since the channel impulse from the transmitter (Tx) to the TE is not constant. The AAOA is able to simulate the angle, but as mentioned previously the lack of control over the side-lobes might give unwanted results.

Contents

Preface

This project report consist of a main paper which can be read on it is own, and fully cover the projects results and method. Broaden explanation of some concepts from the paper can be found in the appendix chapters.

This master thesis follows IEEE citation methodology, where citations is presented with square bracket and a number e.g. "[1]". The presented paper will have it's own literature list and citation index. The remaining report (appendix) follows it's own citation index and literature list.

Aalborg University, June 1, 2023

Mikkel Bengtson
mbengt17@student.aau.dk

Nomenclature

Abbreviation	*Meaning*
AAOA	arbitrary angle of arrival
ADC	analog to digital converter
AoA	angle of arrival
BW	bandwidth
DAC	digital to analog converter
DoA	direction of arrival
DRFM	digital radio frequency memory
FDOA	flexible direction of arrival
FMCW	frequency modulated continues wave
IC	integrated circuits
LOS	Line of Sight
LPF	low pass filter
MIMO	multiple inputs multiple outputs
mmWave	millimeter Wave
NLOS	Non Line of Sight
OTA	over the air
RF	radio frequency
RTS	radar target simulation
RuT	radar under test
Rx	receiver
SIMO	single input multiple outputs
TE	target emulator
Tx	transmitter
ULA	uniform linear array
VAA	virtual antenna array

An Investigation Of Angle-of-Arrival Radar Target Simulation for Automotive Radar

Mikkel Bengtson

Abstract—**Automotive mmWave radar is becoming more accessible,, and is expected to be more widely used in autonomous driving sensor setup. integrated circuits (IC) mmWave radar allows for compact multiple inputs multiple outputs (MIMO) radar designs enabling automotive radars to have angular target estimation. Higher safety standards and increased complexity of radar setup increases the requirements for testing setup. Academia along with the industry are developing radar target simulation (RTS) systems which can handle the new test requirements. The different methodologies for simulating targets are reviewed along with methods for optimizing the simulated targets angle using fewer target emulator (TE) are reviewed. A new flexible method using a superposition of two TE for simulating angle along with a direct modulation technique is presented.**

The new presented method is simulated, showing the capabilities of the method. It was possible to simulated different targets with multiple TEs, however, the technique lacks the control of the side-lobes of the angular response which might result in ghost targets. Simulation of RTS systems is performed for evaluating the two main angular simulation methods, arbitrary angle of arrival (AAOA) and flexible direction of arrival (FDOA) by comparing them to a TE placed at the wanted angle. Precise Reconstruction is possible using the FDOA, however, the method fails when considering MIMO radar system since the channel impulse from the transmitter (Tx) to the TE is not constant. The AAOA is able to simulate the angle, but as mentioned previusly the lack of control over the side-lobes might give unwanted results.

Index Terms—**mmWave, Radar, Radar target simulation, Over the air test**

I. Introduction

With a goal of achieving autonomous driving in the future along with driving assisting systems, extensive sensor systems are developing [1]. Typically LIDAR and camera systems are used along with radars in autonomous driving. Radar systems outperforms LIDAR and camera solution in adverse weather conditions i.e. rain, fog etc. [2]. Radar systems have been used in cars for many year in applications such as rear sensor and parking sensor. Typically these systems consists of single unit sensor, that simply detect a simple distance between the sensor the nearest object [1]. In autonomous driving scenarios, a fast changing environment, consisting of pedestrian, cyclist and other cars increases the complexity of the sensor systems, hence also increasing the required testing systems for safe operation [1].

Continues development over the last decade of systems utilizing the lower mmWave frequency bands from 30-100 GHz, have made single unit transceiver IC utilizing the frequency band available [3], [4]. A big advancement is in the automotive radar industry, doing the last years is cheap ICs operating in the frequency bands from 76 GHz to 81 GHz being available. Having a large bandwidth allows the radars to have good range resolution. With the wavelength being low, antenna arrays can be made in a small form factor, giving the radar the possibilities to have angular resolution along with velocity and distance [5].

Radar target simulation (RTS) are used for testing radars [6]–[9]. Typically radar-in-the-loop testing is wanted, where the sensor is attached to the car, hence the test setup must be an over the air (OTA) solution [10]. RTS works by simulating different targets, with the test device placed at a fixed distance from the radar. Previous RTS systems can typically only simulate a single target, with the angle of arrival (AoA) being that of the TE. Academia along with newest industry test setups are, extending the test capabilities of the RTS systems. Both increases in the amount of simulated targets and the capabilities of simulating different target angles so complex scenarios can be simulated are being developed.

This paper will investigate the current state of RTS systems for typical automotive radars. A review of state-of-the-art commercial and academia advancement in RTS is presented in Section II. With the angle of target being important for testing new mm-Wave radar setups, a review of angular target simulation is done in Section III. A new RTS methodology is proposed in Section III-B, which combines described methods from Section II and Section III-B. A signal model for RTS systems is presented in Section IV, which is the base for comparing the different methods for simulating targets. Results of the simulation are presented in Section V. The new proposed methods simulation results is presented inSection V-A and comparison between the angular methods is presented in Section V-B. Concluding marks are done in Section VI.

II. State of the Art Radar Target Simulator

RTS systems are dedicated systems designed for evaluation and assessing the performance of radar systems. OTA solutions are considered a necessity for in-the-loop test setups, where the radar under test (RuT) is integrated into the application, such as a car. With OTA solutions, evaluation and verification of the radar performances can be tested in real-world scenarios, simulating the actual propagation of electromagnetic signals in the environment.

To effectively test a RuT a RTS systems must be able to simulate the objects, distance, velocity and angle. To address

Mikkel Bengtson with the Antenna Propagation and Millimeter-wave Systems (APMS) section, Aalborg University, Denmark.

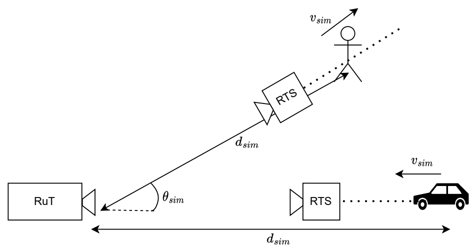

Fig. 1: Illustration of single radar tester. A single RTS front end is only able to simulate range and velocity in a line following the physical angle in respect to the RuT.

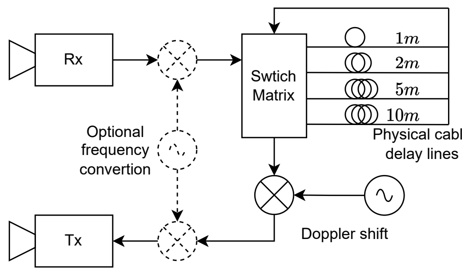

Fig. 2: Principles of delay line solution

the simulating requirements there are different commercial solutions available on the market. In addition to commercial solution, academia have made significant contributions by providing improvements and optimizations of different aspects of RTS. In this chapter current on the market commercial solutions are explored, followed by a summary of the recent state of the art suggestions from academia.

A. Commercial solutions

The commercial solutions can in general be split into 2 different categories: single radar tester and full emulation. Single Radar tester can simulate distance and velocity in a straight line aligned the angle of the RTS as illustrated in Fig. 1. These systems are particularly suitable for testing simple onboard radars for applications such as speed control, parking sensors etc. Where the distance to a single object in a straight line in front of the sensor is the relevant object. Several commercial solutions follow this approach, including ASGARD1, E8718A Radar Target Simulator, dSPACE Automotive Radar Test Systems (DARTS) and R&S®AREG100A automotive radar echo generator [6]–[9]. The inner working of the RTS systems are not described in the companies official documentation, however we can assume they employ some of the methods described later.

The solutions 8718A Radar Target Simulator, dSPACE Automotive Radar Test Systems (DARTS) and R&S AREG100A automotive radar echo generator are quite similar, with the main differences being the amount of front ends a single signal generator can support. Parameters such as the frequency, bandwidth, simulation range, simulation velocity is different from each brand. Choosing the best solution for simulating a particular scenario depends on the RuT and its specific requirements.

Uniquesec ASGARD1 solution stands out from the others, as it offers feature where multiple targets can be generated by a single front-end. However, it should be noted that only a single AoA can simulated, determined by the position of the RTS. The solution only works for frequency modulated continues wave (FMCW) radars, since the solution takes advantages of the specific waveform [11].

The full emulation scene category involves generating a comprehensive and detailed simulated scene for a specific scenario. These solutions are designed for testing and developing of fully autonomous cars, where a complex radar scene is crucial. One example of such solution is Keysight's AD1012A Radar Scene Emulator, which fulfills these requirements by employing a lot of RTS front ends.

In [10] another example of a full emulation scene is presented, using dSPACE Automotive Radar Test Systems solution. Here the RTS system is extended by using front ends mounted on rails such that each front end can be shifted to a specific angle. This solution allows for more complex scenarios since dynamic angles can be simulated. However, the solution is still limited by the amount of targets that can be simulated simultaneously.

B. Academia - State of the art

In general, the literature presents 3 different RTS principles, referred as: delay line solution3, digital solution and direct modulation. Recent research typically focuses on improving these principles to simplify implementation or enhance performance, as detailed below.

1) Delay Line Solution: Delay line solution, uses a tap-delay line to extend the delay (distance) of the signal, by increasing its physical travel [12]–[16]. The signal is captured and then delayed physically using cables, hence simulating a reflection of an object a certain distance away. The velocity of the object is simulated by mixing the signal with a doppler frequency giving the shift corresponding to the velocity of the object. Depending on the carrier frequency of the RuT a frequency shift is typically applied before the the delay lines, to minimize the loss in the cables. In Fig. 2 a principle diagram of the delay line solution is seen.

In [13] a delay line RTS system is presented for 77 GHz automotive radar. By utilizing a splitter in the beginning of the signal chain two targets can be simulated. One target has a fixed distance of 50 m determined by a cable and the second targets distance can be adjusted between 0.5m and 128m via a switch matrix and cables with varying lengths. A similar system is presented in [12], with a single signal line. In this system, instead of using coaxial RF-cables, the signal is converted to optical signals and the delay line is implemented using optical cable. In [16] and [14] a more advanced structure of the switched delay line is proposed. Instead of using a single switch module with different lengths of cable to extend the range, the delay line is implemented as a tapped line. By doing so multiple targets can be generated with a single system. For each tap line a switched structure is used to set a more fine resolution delay.

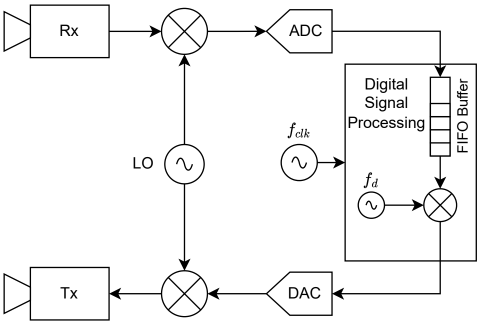

Fig. 3: Principle diagram of digital solution

Alternative methods for implementing the delay line are discussed in [15], including the use of SAW filter, BAW filter, LTCC technology and Lumped element filter to introduce a signal delay which are compared with typical cable structure. Compared to cable structure methods, filters can achieve a more compact and a cost efficient RTS system. Different SAW filters along with "LTCC delay line" was tested by the authors and is suggested for use in a delay line RTS system. However, no real RTS system utilizing the technology is presented in the paper.

2) Digital Solution: Digital solution, uses digital signal processing to generated the simulated radar signals. A principle diagram of the digital solution is seen in Fig. 3. The captured signal is mixed to a lower frequency, effectively lowering the required sampling rate. The signal is then sampled by an analog to digital converter (ADC). Different signal processing methods can be used for simulating the target. After the signal has been processed to simulate a target the signal, it is converted back to an analog signal by a digital to analog converter (DAC). Finally the signal is mixed with the carrier frequency converting it back to the original frequency range of the RuT [17]–[22].

To simulate distance in the digital solution, a simple FIFO buffer is typically used. The FIFO buffer delays the signal in steps corresponding to the clock frequency, which sets the lowest difference in distance. This method is also called digital radio frequency memory (DRFM). The velocity can be implemented by mixing the signal with the desired doppler frequency in the digital domain.

In [17] a digital RTS system is demonstrated. They are able to simulate targets with a minimum distance of 16 m, limited by the sampling speed of the ADC and DAC. In the tested system, a ghost target can be observed from spurious frequency caused by imbalance in the I-Q in the up and down conversion.

A different doppler frequency method is proposed in [18], where direct frequency synthesis is used. The principle is to attenuate the samples of the signal based on a lookup phase table. However, the method suffers from periodic spurious frequencies. To combat this the author alternates the signal by adding a small phase jitter.

Multirate sampling is used in [19]–[21] to introduce doppler shift for simulation of the velocity. In [19] the fundamentals of the method is described. By introducing a difference in the sampling frequency of the ADC and the synthesis frequency of the DAC, a doppler shift can be synthesised. The authors compare the multirate method with DRFM and observe an improvement in attenuating unwanted frequencies in the doppler domain. In [21] the system is expanded to include frequency multipliers/dividers so the system can handle carrier frequencies up to 77GHz. To lower the steps in the signal chain to obtain an IF for sampling [20] investigates how sampling the signal at a higher nyquist zone can be used. A demonstration of sampling the signal at a higher IF-frequency was demonstrated, however the noise floor in the distance domain was raised by 10 dB.

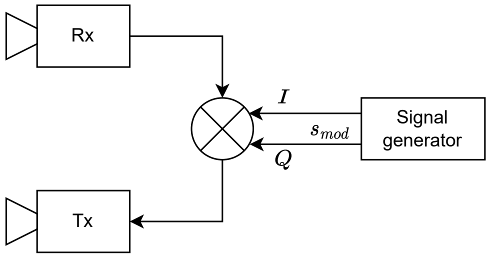

Fig. 4: Principle diagram of direct modulation solution

In [22], a fractional delay filter is used to be enable the simulation of delays (distances) and velocities that do not align with the sampling frequency.

3) Direct modulation: In direct modulation, the waveform of FMCW radars is used to generate the simulated target. By mixing the transmitted signal from the RuT with a specified signal such that the demodulated signal at the RuT will be detected as a target [11], [23]–[29]. For a direct modulation to work, knowledge of the FMCW waveform, such as the bandwidth (BW), chirp time T_c and distance between the RuT and RTS must be available. Modulation signal which is mixed with the received signal at the RTS as shown in Fig. 4 is given by Equation (1)[23].

$$s_{mod}(t) = \exp\left(j2\pi\frac{BW}{T_c}(\tau_{sim} - \tau)t + \phi_{0,mod}(t)\right) \quad (1)$$

Where τ is the time for the signal to travel between the RTS and RuT, and τ_{sim} is the delay for the simulated target. The phase term $\phi_{0,mod}(t)$ sets the slow rotating doppler shift.

A low cost RTS component utilizing the direct modulation is presented in [23], [24]. The authors demonstrate a simple design using only a diode, along with the physical tracing for a PCB for modulating the signal from the RuT. Thought external signal generation for generating the signal presented in Equation (1) is required. The authors argue that having low cost TEs, multiple angles can easily be simulated with physical placement of the TE at the wanted angles.

The direct modulation method is used in [26], [27], [30] for simulating micro Doppler's from pedestrians and cyclist. They successfully demonstrates the systems ability to simulate previously measured micro-doppler signatures. It is shown by [28] that an estimator unit can be used along with the modulation, to estimate the FMCW parameters. The effect of hardware non-idealities for a direct modulation is investigated

TABLE I: Comparison of the different RTS system principles

Method	Pros	Cons	Ref.
Delay line solution	+Works with every waveform +Minimum distance is from RuT to TE +Principle is simple	-Fixed distance -Complex setup for multiple distances -Setup requires lot of cable/space -Can only simulate a single target	[12]–[16]
Digital solution	+Works with every waveform +Easy to simulate different distances	-Require high samplerate/clockrate -Minimum distance is high $< 10\,m$	[17]–[22]
Combined Digital and delay line	+Works with every waveform +Minimum distance is from RuT to TE +Works with every waveform	-System gets complex -"Digital" targets might differ from "delayline"	
Direct modulation	+Any distance/velocity +Can simulate multiple targets with single TE	-Only works for FMCW -Requires waveform parameters	[11], [23]–[29]

in [29], which shows that some ghost targets might appear from harmonics of the modulated signal.

C. Comparison

In Table I, pros and cons of the three different RTS principles are summarized and compared. Delay line, digital, and combined delay line with digital methods offer the advantages of being adaptable to different types of waveforms. Since the methods do not depend on the specific properties of the signal. If the test setup is required for testing many different radars or radars with unknown waveform those methods are preferred. However, the methods lacks the ability to simulate multiple target simultaneously, unlike the direct modulation. With the ability to simulate multiple targets, fewer TE are required to achieve a more complex simulation scenario.

III. State of the art - Angle Simulation

Simulating the angle of a target is important for more complex new radar systems. In general two approaches can be used. The angle is obtained by either mechanically placed antennas or by using signal processing techniques.

As mentioned in Section II, Keysights AD1012A Radar Scene Emulator achieves a angular simulation by mechanically allocating many TE to predefined positions [31]. Mechanically moving the TE is also a possibility as explored in [10]. However, moving the TE limits the amount of targets that can be simulated simultaneously and therefore also the complexity of the simulated scene.

Recently two different methods have been proposed to simulate detailed angles of targets using fewer antennas [32]–[34]. A brief description of the methods will be provided below. By simulating the RTS systems based on the two methods a comparison is made in Section V.

A. Flexible Direction of Arrival (FDOA)

Flexible direction of arrival (FDOA) can emulate targets with arbitrary directions of arrival based on knowledge of the propagation channel between the Tx port, TE and receiver (Rx) port [33]. The method assumes a narrow-band channel model, hence the propagation distance gives a phase-shift depending on the total travel distance of the wave $d_{Tx,Ten} + d_{Tem,Rxm}$. For the sake of simplicity, we assume the number of TE N and Rx antenna ports M are identical resulting in a square matrix $\mathbf{C_{n,m}}$ consisting of the channel response. Hence the following signal model can be derived.

$$s_{rx,m}(t) = \mathbf{C_{m,n}} s_{mod,n} s_{tx}(t) \tag{2}$$

Where $s_{rx,m}(t)$ is the received signal at Rx antenna port m. $s_{mod,n}$ is the modulation vector where each row n corresponds to a TE. The modulation vector is constructed based on the direct modulation technique, along with controlling the phase the each of the individual ports in such a way that the RuT experiences an incident wave from a specific direction. By multiplying the modulation vector with the inverse channel matrix $C_{m,n}^{-1}$, given the channel matrix $C_{m,n}$ is invertible. The received signal will directly be a product of the modulation vector and the transmitted signal.

$$s_{rx,m}(t) = \mathbf{C_{m,n}} \mathbf{C_{m,n}}^{-1} \mathbf{s_{mod,n}} s_{tx}(t) = \mathbf{I}\, \mathbf{s_{mod,n}} s_{tx}(t) \tag{3}$$

With $\mathbf{I}$ being an identity matrix. The locations of the TE should be properly designed for achieving a good-conditioned channel matrix as described in the paper [33]. Since the direct modulation method is used, method should be able to simulate any target.

B. Arbitrary Angle of Arrival (AAOA)

The AAOA method relies on the principles that the RuT cannot distinguish signals from two TE if the angle between them is smaller than the angle resolution of the radar. By properly allocating TEs and assigning weights to them, an arbitrary angle of the target within the angular range covered by the two TEs can be emulated. Furthermore, the signal received from the two TE must be detected in the same velocity and range bin. The signal received by the RuT is thereby the superposition of the signals from the two TEs and creates the illusion of a target at a specific direction [32].

Given the AAOA method the amplitude ratio between the signal from Te_1 and Te_2 can be calculated as [32].

$$\frac{A_1}{A_2} = -\frac{g_2(\alpha)}{g_1(\alpha)} \tag{4}$$

Where

$$g_{te}(\alpha) = \frac{2\cos(\alpha)\sin\left(\pi\frac{N_{rx}}{2}\left(\sin(\theta_{te}) - \sin(\alpha)\right)\right)}{\pi N_{rx}\left(\sin(\theta_{te}) - \sin(\alpha)\right)^2} - \frac{\cos(\alpha)\cos\left(\pi\frac{N_{rx}}{2}\left(\sin(\theta_{te}) - \sin(\alpha)\right)\right)}{\sin(\theta_{te}) - \sin(\alpha)} \tag{5}$$

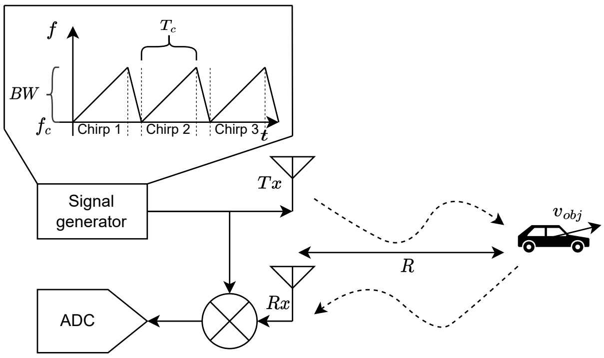

Fig. 5: Illustration of FMCW radar.

Where α is the desired simulated angle, θ_{te} is the angular location of the TE in relation to the RuT, N_{rx} is the number of receive antennas. The authors of [32] extend the method for simulating angle in both elevation and azimuth in [34].

The method is in general compatible of working with any RTS method. In [32], [34] a digital solution is used to demonstrate the methods capabilities. In this paper the direct modulation method along with the AAOA method is proposed which demonstrates that the direct modulation multiple targets can be generated with a single TE. Based on the signal simulation model described in Section IV, the feasibility of using AAOA with direct modulation is shown in Section V-A.

The signal from two TEs with an angular spacing less then the resolution of the radar can simulate an arbitrary angle between the two TEs discussed above, when the modulation signal of the two TEs are designed as:

$$s_{mod,te1}(t) = A_1 \exp\left(j2\pi \frac{BW}{T_c}(\tau_{sim} - \tau)t + \phi_{0,mod}(t)\right) \tag{6}$$

$$s_{mod,te2}(t) = A_2 \exp\left(j2\pi \frac{BW}{T_c}(\tau_{sim} - \tau)t + \phi_{0,mod}(t)\right) \tag{7}$$

With A_1 and A_2 being the ratio defined in Equation (4) and $\phi_{0,mod}(t)$ being the slow varying phaseshift corresponding to the dopplershift caused by the object. Multiple targets with different velocities and distances can then be simulate by the same two TEs. The angles of the multiple targets generated by the same TE pair can vary as velocity and distance change. Hence, the method should be able to simulate a large amount of targets using relatively few TEs.

IV. Signal model for simulation

The signal model is based on FMCW radar. The transmitted signal from the radar, follows a linear frequency sweep with a start frequency f_c, whoese instantenous frequency is given as [35].

$$f_{tx}(t) = f_c + \frac{BW}{T_c}\, t \tag{8}$$

Hence the phase, of the transmitted signal is found by integrating the frequency sweep over time.

$$\phi_{tx}(t) = 2\pi \int_0^t f_{tx}(t)dt = 2\pi \left(f_c t + \frac{1}{2}\alpha t^2\right) \tag{9}$$

With $\alpha = \frac{BW}{T_c}$, BW the sweep bandwidth and T_c the sweep period. If the transmitted signal hits an object at a distance R away from the radar, the received signal will be time delayed due to the travel time of the signal. With the time delay denoted by τ, the phase of the received signal can thereby be given as:

$$\phi_{rx}(t) = 2\pi \left(f_c(t-\tau) + \frac{1}{2}\alpha(t-\tau)^2\right) \tag{10}$$

Via mixing the received signal with the transmitted signal, the phase difference between them can be extracted as

$$\Delta\phi(t) = \phi_{rx}(t) - \phi_{tx}(t) = 2\pi \left(-f_c\tau - \alpha t\tau + \frac{1}{2}\alpha\tau^2\right) \tag{11}$$

The last term is typically removed since the phase contribution is minimal [36]. Assuming a moving object, its delay is dependent on the speed v_{obj} and distance R of the target, i.e. $\tau = \frac{2(R+v_{obj}t)}{c}$ with c being the speed of light. The phase difference in Equation (11) can thereby be given as:

$$\Delta\phi(t) = 2\pi \left(-f_c \frac{2(R+v_{obj}t)}{c} - \alpha t \frac{2(R+v_{obj}t)}{c}\right) \tag{12}$$

Letting $\tau_{obj} = \frac{2\,R}{c}$ and $f_d = f_c\,\frac{2v_{obj}}{c}$ the equation can be rewritten

$$\Delta\phi_{rx}(t) = 2\pi \left(-f_c\tau_{obj} - tf_d - \alpha t\tau_{obj} - \alpha t^2 \frac{2v_{obj}}{c}\right) \tag{13}$$

The contribution of the last term is neglectable and is therefore typically removed [36]. The signal is sampled with sample frequency f_s

$$x[n_r] = A\exp(j\phi_{rx}\left(\frac{n_r}{f_s}\right)) \tag{14}$$

Where A is the amplitude of the sampled signal. A fast sweep multiple chirp signal waveform is assumed. Hence the Chirp is repeated with a period $T_P = T_c + T_d$ where T_d is the period between to chirps [35], [37]. The two dimensional signal, with $m_v \in [0, M_v - 1]$, being the chirp index from 0 to the number of chirps M is given as

$$x_{2D}[n_r, m_v] = A\exp\left(j2\pi\left(-f_c\tau_{obj} - f_d\frac{n_r}{f_s}m_vT_p - \alpha\tau_{obj}\frac{n_r}{f_s}m_vT_p\right)\right) \tag{15}$$

A two dimensional discrete fourier transform (DFT) over the chirps, and the samples is performed

$$X_{2D}[f_R, f_v] = \sum_{m_v=0}^{M_v}\sum_{n_r=0}^{N_r-1} x_{2D}[n_r, m_v] \exp\left(-j2\pi\frac{n_r\,f_R}{N_r}\right)\exp\left(-j2\pi\frac{m_v\,f_v}{M_v}\right) \tag{16}$$

The doppler shift term $f_d\frac{n_r}{f_s}m_vT_p$ can be seen as constant over the range DFT hence a frequency at $\alpha\tau_{obj}$ will be seen. For each constant range bin, the second DFT will have a changing phase over the chirps and hence a frequency peak corresponds to the doppler frequency for the speed of the object [38].

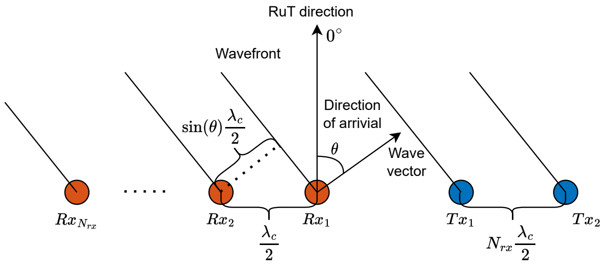

Fig. 6: Illustration of MIMO radar setup using virtual antenna arrays.

Hence by peak search in the 2D-frequency domain (i.e. range and doppler drequency domain) of the signal, objects can be detected.

A. Angular estimation

Automotive FMCW IC uses MIMO configuration to enable angular estimation of the objects, the setup is illustrated in Fig. 6. A phase shift between each Rx is determined by to the AoA of the reflected wave. Returning to Equation (14) and assuming that the delay τ_{obj} is the distance to the first element, there will be an additional phase shift for each Rx element. Assuming the distance between the elements is $\frac{\lambda_c}{2}$, the received signal at antenna element $p_a \in [0, P_A - 1]$ is: [38], [39]

$$x[n_r, p_a] = x[n_r] \exp\left(-j\pi \sin(\theta)\, p_a\right) \tag{17}$$

Where θ is the angle of the incoming reflected wave, i.e. direction of arrival (DoA). Given a certain angle θ, a linear change in phase over the P elements can be viewed as a frequency. Extending Equation (15) with the linear antenna array we have:

$$\begin{aligned} x_{3D}[n_r, m_v, p_a] = A \exp\Bigg[j2\pi \bigg(-f_c\tau_{obj} - f_d \frac{n_r}{f_s} m_v T_p \\ -\alpha\tau_{obj}\frac{n_r}{f_s} m_v T_p \bigg) - j\pi \sin(\theta)\, p_a \Bigg] \end{aligned} \tag{18}$$

A 3-dimensional DFT is performed with the third dimension representing the angular frequency domain i.e.

$$\begin{aligned} X_{3D}[f_R, f_v, f_a] = \sum_{p_a=0}^{P_a-1} \sum_{m_v=0}^{M_v-1} \sum_{ns=0}^{N_s-1} x_{3D}[n_r, m_v, p_a] \\ \exp\left(-j2\pi \frac{n_r\, f_R}{N_r}\right) \exp\left(-j2\pi \frac{m_v\, f_v}{M_v}\right) \exp\left(-j2\pi \frac{p_a\, f_a}{P_a}\right) \end{aligned} \tag{19}$$

To improve the angular resolution, multiple Tx antennas can be used. A virtual antenna array is constructed by utilizing the co-located Tx and Rx. By locating Q Tx antenna with a distance of $P_a\, d$ apart from the first Tx antenna, a virtual antenna array composed of $Q \cdot P_a$ elements can be realized [39].

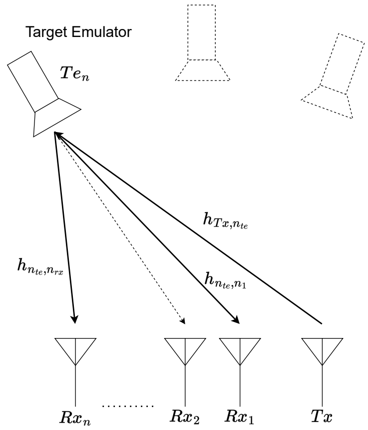

Fig. 7: Illustration of channel between RuT and TE

B. Radar target simulation signal model

In a radar target simulation setup with a MIMO radar, a number of TE is positioned at a distance D and angle β from the RuT as illustrated in Fig. 7. The signal from the Tx antenna will travel to all the TE giving the outgoing channel matrix $C_{Tx,Te}$.

$$C_{tx,te} = \begin{bmatrix} h_{Tx,n} & \cdots & 0 \\ \vdots & \ddots & \vdots \\ 0 & \cdots & h_{Tx,N_{Te}} \end{bmatrix} \tag{20}$$

With L_tx, n and τ_tx, n denoting the path loss and delay, respectively, caused by the traveling of the signal from Tx to the n-th TE, the channel impulse response between the Tx and the n-th TE can be given as:

$$h_{tx,n} = L_{Tx,n}\, \delta(t - \tau_{Tx,n}) \tag{21}$$

From each TE to each Rx antenna the channel matrix can be expressed as:

$$C_{te,rx} = \begin{bmatrix} h_{n_{te},n_{rx}} & \cdots & h_{1,N_{Rx}} \\ \vdots & \ddots & \vdots \\ h_{N_{Te},1} & \cdots & h_{N_{Te},N_{Rx}} \end{bmatrix} \tag{22}$$

With the coefficients given by:

$$h_{n_{te},n_{rx}} = L_{n_{te},n_{rx}}\, \delta(t - \tau_{n_{te},n_{rx}}) \tag{23}$$

The received signal can thereby be written as

$$s_{rx}(t) = C_{te,rx} * (C_{tx,te} * s_{tx}(t))\, s_{mod}(t) \tag{24}$$

V. RESULTS

Based on the above signal model, numerical simulations have been performed. Results of simulating the extended AAOA is presented in Section V-A. The results of simulating both the AAOA and the FDOA with same radar parameters and same targets is presented in Section V-B. For both simulation the same RuT parameters are set and are summarized in Table III. A BW of 4 GHz, a carry frequency $f_c = 79$ GHz, and a sweep period of 40 μs are set for the RuT for both simulations. However, antenna setup is different for each simulation.

TABLE II: Simulated target for simulating multiple targets using AAOA and direct modulation

Highlight	#	Dist. [m]	Vel. [m/s]	Angle
Single target	1	5	5	$-15°$
Same angle, different distance and velocity	2	10	5	$-5°$
	3	15	0	$-5°$
Narrow angle same distance and velocity	4	15	-5	$5°$
	5	15	-5	$15°$
Wide angle same distance and velocity	6	5	-7	$-6°$
	7	5	-7	$18°$

A. *Extension of Arbitrary Angle of Arrival*

The AAOA with the direct modulation technique, called extended AAOA forward, is used to simulate multiple targets simultaneously and compared with a baseline. For the baseline the TE is placed at the desired angle. Seven targets are simulated which highlights the different properties of the technique, the simulated target values can be seen in Table II. The Tx is composed of 1 antenna and the Rx of 4 antennas. The element spacing of the Tx is $2\lambda_c$ and the Rx element spacing is $\lambda_c/2$.

After performing the 3D DFT to the received signal a distance-velocity profile can be obtained as plotted in Fig. 8, for the baseline and AAOA simulation respectively All the distance-velocity pairs are highlighted for both the baseline, and AAOA. Some targets, e.g., 6 and 7, are located at identical distance-velocity. Comparing the baseline Fig. 8a with the AAOA Fig. 8b the same simulated objects can be detected at the same velocity distance bins. The main difference between the two is the gain at the individual peaks. For the targets with the same velocity and distances while with different angles, the angular plots at the given distance-velocity bins are shown in Fig. 8 for target pairs 4 & 5 and 6 & 7, respectively

A comparison plot between the extended AAOA and the baseline is shown in Fig. 8a, for the targets pair 4 & 5, where the angular profiles are matched well and only one peak can be observed at this bin, suggesting that the RuT is not able to distinguish the directions of the two target. Since the angular interval between these two targets is smaller than the angular resolution $\alpha_{res} \approx 15°$ of the Rx antenna array [39]. In Fig. 9b two peaks can be seen in the angular profile, due to that, the simulated angle between the two targets is larger than the angular resolution. However, we can observe that the angular profile of the extended AAOA method defers from the baseline with a significant power drop at $18°$. On both the baseline and the extended AAOA, a high side lobe is observed. The peak are from the superposition of the side lobes of the angular response. The angular response is similar between the baseline and the extended AAOA in both Fig. 9a and Fig. 9b, based on the requirement of the test for RuT the method might be valid for use.

B. *Comparison between AAOA and FDOA*

A test with a MIMO setup simulating multiple angles at the same distance velocity is shown in Fig. 10. Four targets angular spaced larger then the minimum resolution of the RuT is simulated. From the resulting angular magnitude response, it can be seen that the reference should be able to identify

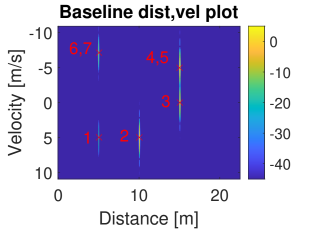

(a) Baseline simulation, with the TE placed at the angles shown in Table II, the velocity and distance is simulated using direct modulation.

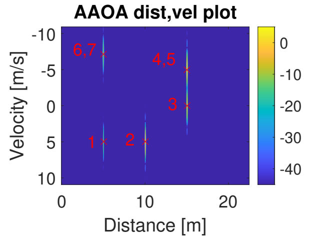

(b) AAOA with direct modulation simulation, with the TE placed at $-20°$, $-10°$, $0°$, $10°$, $20°$. The simulated are set in II.

Fig. 8: Normalized distance-velocity plot, for baseline and AAOA angle simulation.

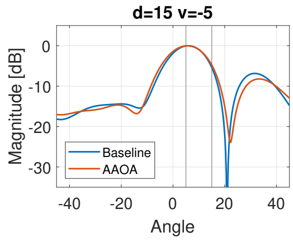

(a) Angle plot at a distance 15 m and -5 m/s corresponding to target #4 and #5. The black lines corresponds to the target angles $5°$ and $15°$

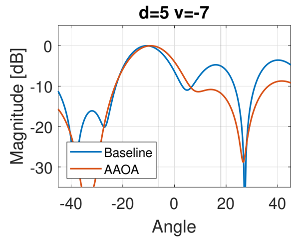

(b) Angle plot at a distance 5 m and -7 m/s corresponding to target #6 and #7. The black lines corresponds to the target angles $-6°$ and $18°$

Fig. 9: Angle plot at two different distance, velocity bins.

two separate targets. The AAOA is not able to simulate a wanted angular response, this is mainly due to superposition of the side-lobes from the different angular response from the individual TEs. The FDOA is able to simulate 4 distinct targets, simulated targets are more separated in the angular spaced compared to the desired ones.

A comparison between the AAOA and FDOA, a simulation is performed using both. A target angle of $-5°$ is simulated using, AAOA, FDOA and a reference where the TE is placed at the target angle. The results can be seen in Fig. 11. In Figures 11a to 11c each individual angle response is showed. The response from each TE is shown with dashed lines, and the superposition, i.e. resulting response is shown with black curves. For the AAOA the angle is simulated using the superposition of two TE, where the FDOA utilizes multiple TE and the combined signal from all TE gives the wanted angle. The the angular responses obtained with different methods shown in Fig. 11 are similar. The the main beam lobe as well as

TABLE III: RuT simulation parameters

Parameter	Value
Carry frequency f_c	$79GHz$
Bandwidth BW	$4GHz$
Sweep period T_c	40 μs
Number of Chirps M_v	32
Number of Rx	4
Number of Tx	2

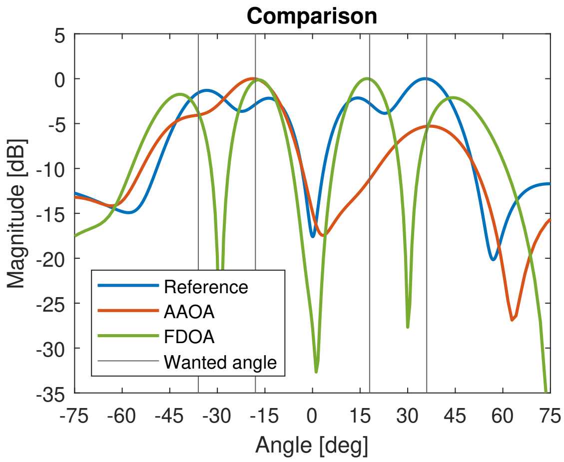

Fig. 10: Comparison of multiple angles

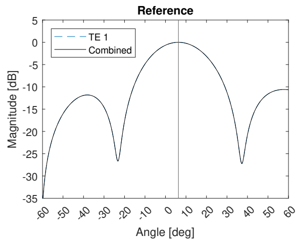

(a) Reference by placing a TE at the angle.

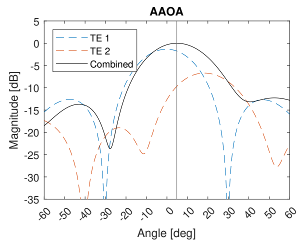

(b) Arbitrary angle of arrival (AAOA) using 2 TEs placed at 0 and 15 degrees.

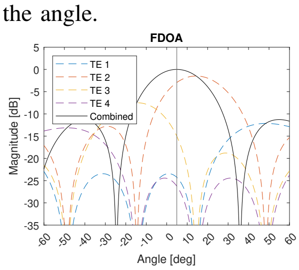

(c) Flexible direction of arrival (FDOA) using 4 TE placed at optimal angles ($-48°$,$-14°$,$14°$,$48°$).

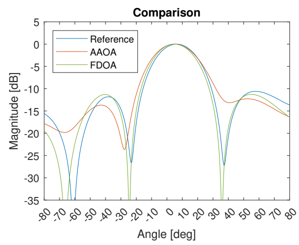

(d) Comparison between reference, Arbitrary angle of arrival and flexible direction of arrival

Fig. 11: Angle simulation by, using the different methods. Target angle is $-5°$, a 4 element uniform linear array (ULA) at the Rx is used with a single Tx. The dashed line is the signal from each TE.

the side lobes of the AAOA method are slightly different from the reference and FDOA. Since the method only optimizes for the main lobe to achieve the wanted angle, without control of the side lobes. The FDOA have a similar angle response to the reference and is mainly different in the null location further away from the targeted angle.

VI. Conclusion

A review of different approaches for target emulation have been investigated. The different methodologies have different pros and cons. The direct modulation method is promising since it allows for arbitrary amount of targets to be generated with a single TE unit. The method however, is only able to work with FMCW waveform and the parameters of the RuT must be known in advance. A combination of the digital solution and delay line solution can offer a more comprehensive and flexible RTS system. Since the target is emulated by directly delay the actual signal, along with applying an actual doppler shift.

Extending the AAOA with the direct modulation, promising simulation results can be acheived. However, care must be taken in regards to the side-lobes if multiple targets at close angles must be simulated. The side-lobes of the superposition from multiple TE can effect the perceived angle of the target and make the RuT see ghost targets. For full validation of the method, actual system test must be performed and the methodology must be validated with physical measurements.

Both the AAOA and FDOA can be used for simulating targets at different angular position when the RuT uses a single input multiple outputs (SIMO) setup. The FDOA is not capable of making a simulation setup when the RuT have multiple Tx antennas. The channel response is changing when the RuT goes from transmitting from one Tx to the other. Hence the matrix inversion is problematic. Further, investigation must be performed if a methodology utilizing the inverse channel is to be used for MIMO systems.

Acknowledgment

A thanks to Wei Fan and Fengchun Zhang for supervision.

References

[1] C. Waldschmidt, J. Hasch, and W. Menzel, “Automotive Radar — From First Efforts to Future Systems,” *IEEE Journal of Microwaves*, vol. 1, no. 1, pp. 135–148, 2021. DOI: 10.1109/JMW.2020.3033616.

[2] Keysight, “How Millimeter Wave Automotive Radar Enhances Advanced Driver Assistance Systems (ADAS) and Autonomous Driving,” Keysight, Tech. Rep., 2023.

[3] J. Lee, Y.-A. Li, M.-H. Hung, and S.-J. Huang, “A Fully-Integrated 77-GHz FMCW Radar Transceiver in 65-nm CMOS Technology,” *IEEE Journal of Solid-State Circuits*, vol. 45, no. 12, pp. 2746–2756, 2010. DOI: 10.1109/JSSC.2010.2075250.

[4] V. Winkler, R. Feger, and L. Maurer, “79GHz automotive short range radar sensor based on single-chip SiGe-transceivers,” in *2008 European Radar Conference*, 2008, pp. 459–462. DOI: 10.1109/EUMC.2008.4751781.

[5] J.-J. Lin, Y.-P. Li, W.-C. Hsu, and T.-S. Lee, “Design of an FMCW radar baseband signal processing system for automotive application,” *SpringerPlus*, vol. 5, Dec. 2016. DOI: 10.1186/s40064-015-1583-5.

[6] Uniquesec, *ASGARD1*, http://web.archive.org/web/20080207010024/http://www.808multimedia.com/winnt/kernel.html, Accessed: 28-03-2023.

[7] dSPACE, *dSPACE Automotive Radar Test Systems (DARTS)*, https://www.dspace.com/en/pub/home/products/systems/darts.cfm#180_45183, Accessed: 28-03-2023.

[8] Keysight, *E8718A Radar Target Simulator*, https://www.keysight.com/us/en/product/E8718A/radar-target-simulator-76-81ghz-remote-front-end.html, Accessed: 28-03-2023.

[9] Rhode & Schwartz, *R&S®AREG100A automotive radar echo generator*, https://www.rohde-schwarz.com/us/products/test-and-measurement/echo-generators/rs-areg100a-automotive-radar-echo-generator_63493-486080.html, Accessed: 28-03-2023.

[10] S. Buddappagari, M. Asghar, F. Baumgärtner, *et al.*, "Over-the-Air Vehicle-in-the-Loop Test System for Installed-Performance Evaluation of Automotive Radar Systems in a Virtual Environment," in *2020 17th European Radar Conference (EuRAD)*, 2021, pp. 278–281. DOI: 10.1109/EuRAD48048.2021.00078.

[11] F. Rafieinia and K. Haghighi, "ASGARDI: A Novel Frequency-based Automotive Radar Target Simulator," in *2020 IEEE MTT-S International Conference on Microwaves for Intelligent Mobility (ICMIM)*, 2020, pp. 1–4. DOI: 10.1109/ICMIM48759.2020.9299008.

[12] M. Engelhardt, F. Pfeiffer, and E. Biebl, "A high bandwidth radar target simulator for automotive radar sensors," in *2016 European Radar Conference (EuRAD)*, 2016, pp. 245–248.

[13] S. Lutz, C. Erhart, T. Walte, and R. Weigel, "Target simulator concept for chirp modulated 77 GHz automotive radar sensors," in *2014 11th European Radar Conference*, 2014, pp. 65–68. DOI: 10.1109/EuRAD.2014.6991208.

[14] A. Gruber, M. Gadringer, H. Schreiber, *et al.*, "Highly scalable radar target simulator for autonomous driving test beds," in *2017 European Radar Conference (EURAD)*, 2017, pp. 147–150. DOI: 10.23919/EURAD.2017.8249168.

[15] F. Arzur, M. Le Roy, A. Pérennec, G. Tanné, and N. Bordais, "Hybrid architecture of a compact, low-cost and gain compensated delay line switchable from 1 m to 250 m for automotive radar target simulator," in *2017 European Radar Conference (EURAD)*, 2017, pp. 239–242. DOI: 10.23919/EURAD.2017.8249191.

[16] M. E. Gadringer, H. Schreiber, A. Gruber, *et al.*, "Virtual reality for automotive radars," *e & i Elektrotechnik und Informationstechnik*, vol. 135, no. 4, pp. 335–343, 2018. DOI: 10.1007/s00502-018-0620-9.

[17] J. Sobotka and J. Novak, "Digital Vehicle Radar Sensor Target Simulation," in *2020 IEEE International Instrumentation and Measurement Technology Conference (I2MTC)*, 2020, pp. 1–5. DOI: 10.1109/I2MTC43012.2020.9129555.

[18] J. Zhang, L. Zhang, P. Gao, and F. Shen, "An FPGA based real-time radar target simulator with high spur suppression," in *2020 15th IEEE International Conference on Signal Processing (ICSP)*, vol. 1, 2020, pp. 126–130. DOI: 10.1109/ICSP48669.2020.9320950.

[19] G. Körner, M. Hoffmann, S. Neidhardt, M. Beer, C. Carlowitz, and M. Vossiek, "Multirate Universal Radar Target Simulator for an Accurate Moving Target Simulation," *IEEE Transactions on Microwave Theory and Techniques*, vol. 69, no. 5, pp. 2730–2740, 2021. DOI: 10.1109/TMTT.2021.3060817.

[20] G. Körner, C. Birkenhauer, P. Stief, C. Carlowitz, and M. Vossiek, "Frequency Extension Method for Multirate Radar Target Simulation Systems," in *2022 14th German Microwave Conference (GeMiC)*, 2022, pp. 116–119.

[21] G. Körner, C. Birkenhauer, P. Stief, C. Carlowitz, and M. Vossiek, "Efficient Bandwidth Enhanced Multirate Radar Target Simulation," in *2022 IEEE/MTT-S International Microwave Symposium - IMS 2022*, 2022, pp. 534–537. DOI: 10.1109/IMS37962.2022.9865650.

[22] A. Diewald, T. Antes, B. Nuss, and T. Zwick, "Implementation of Range Doppler Migration Synthesis for Radar Target Simulation," in *2021 IEEE 93rd Vehicular Technology Conference (VTC2021-Spring)*, 2021, pp. 1–5. DOI: 10.1109/VTC2021-Spring51267.2021.9448793.

[23] W. Scheiblhofer, R. Feger, A. Haderer, and A. Stelzer, "A low-cost multi-target simulator for FMCW radar system calibration and testing," in *2017 European Radar Conference (EURAD)*, 2017, pp. 343–346. DOI: 10.23919/EURAD.2017.8249217.

[24] W. Scheiblhofer, R. Feger, A. Haderer, and A. Stelzer, "Low-cost target simulator for end-of-line tests of 24-GHz radar sensors," in *2018 22nd International Microwave and Radar Conference (MIKON)*, 2018, pp. 531–534. DOI: 10.23919/MIKON.2018.8405277.

[25] A. R. Diewald and C. Culotta-López, "Concepts for radar target simulation," in *Loughborough Antennas & Propagation Conference (LAPC 2017)*, 2017, pp. 1–5. DOI: 10.1049/cp.2017.0229.

[26] J. Iberle, M. A. Mutschler, P. A. Scharf, and T. Walter, "A Radar Target Simulator Concept for Close-Range Targets with Micro-Doppler Signatures," in *2019 12th German Microwave Conference (GeMiC)*, 2019, pp. 198–201. DOI: 10.23919/GEMIC.2019.8698149.

[27] J. Iberle, P. Rippl, and T. Walter, "A Radar Target Simulator for Generating Synthesised and Measured micro-Doppler-Signatures of Vulnerable Road Users," in *2020 17th European Radar Conference (EuRAD)*, 2021, pp. 218–221. DOI: 10.1109/EuRAD48048.2021.00063.

[28] P. Schoeder, B. Schweizer, A. Grathwohl, and C. Waldschmidt, "Multitarget Simulator for Automotive Radar Sensors With Unknown Chirp-Sequence Modulation," *IEEE Microwave and Wireless Components Letters*, vol. 31, no. 9, pp. 1086–1089, 2021. DOI: 10.1109/LMWC.2021.3088882.

[29] P. Schoeder, A. Martin, B. Meinecke, D. Werbunat, and C. Waldschmidt, "A Modulation-Based Radar Target Simulator and Its Hardware Nonidealities," in *2022 19th European Radar Conference (EuRAD)*, 2022, pp. 1–4. DOI: 10.23919/EuRAD54643.2022.9924830.

[30] J. Iberle, M. A. Mutschler, P. A. Scharf, and T. Walter, "A Radar Target Simulator for Generating Micro-Doppler-Signatures of Vulnerable Road Users," in *2019 16th European Radar Conference (EuRAD)*, 2019, pp. 17–20.

[31] *Radar Scene Emulator - Data sheet*, Keysight, Jun. 2021.

[32] A. Diewald, B. Nuss, M. Pauli, and T. Zwick, “Arbitrary Angle of Arrival in Radar Target Simulation,” *IEEE Transactions on Microwave Theory and Techniques*, vol. 70, no. 1, pp. 513–520, 2022. DOI: 10.1109/TMTT.2021.3106268.

[33] P. Schoeder, V. Janoudi, B. Meinecke, D. Werbunat, and C. Waldschmidt, “Flexible Direction-of-Arrival Simulation for Automotive Radar Target Simulators,” *IEEE Journal of Microwaves*, vol. 1, no. 4, pp. 930–940, 2021. DOI: 10.1109/JMW.2021.3103647.

[34] A. Diewald, B. Nuss, J. Galinsky, and T. Zwick, “Two-Dimensional Arbitrary Angle of Arrival in Radar Target Simulation,” in *2022 23rd International Radar Symposium (IRS)*, 2022, pp. 25–29. DOI: 10.23919/IRS54158.2022.9905069.

[35] N. Levano and E. Mozeson, *Radar Signals*. John Wiley & Sons, 2004, ISBN: 978-0-471-47378-7.

[36] V. Winkler, “Range Doppler detection for automotive FMCW radars,” in *2007 European Microwave Conference*, 2007, pp. 1445–1448. DOI: 10.1109/EUMC.2007.4405477.

[37] Z. Tong, R. Renter, and M. Fujimoto, “Fast chirp FMCW radar in automotive applications,” in *IET International Radar Conference 2015*, 2015, pp. 1–4. DOI: 10.1049/cp.2015.1362.

[38] C. Lovescu and S. Rao, “The fundamentals of millimeter wave radar sensors,” Texas Instruemnts, Tech. Rep., 2020.

[39] S. Rao, “MIMO Radar,” Texas Instruemnts, Tech. Rep., 2018.

A Appendix

A.1 Extended Signal Model

A frequency modulated continues wave (FMCW) waveform, covers a bandwidth (BW) by sweeping the frequency over time also called a CHIRP. The signal starts at a carry frequency f_c covering a BW B over time T_c, illustrated in figure A.1.

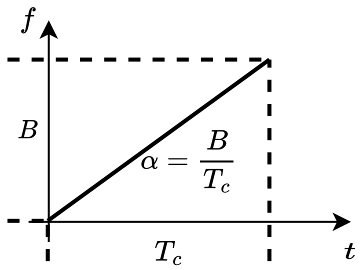

Figure A.1: Illustration of frequency over time for a CHIRP signal also called a linear FMCW signal.

Different frequency functions may be used to modulate the frequency over time, each alters the waveform properties. In typical industry standard FMCW IC for automotive and industrial applications a standard linear sweep is used, where the frequency increases or decreases linear with time [1]. For the up-chirp, increase in frequency over time, the frequency function can be written as.

$$f(t) = f_c + \alpha t \tag{A.1}$$

Where f_c is the carry frequency, $\alpha = B/T_c$ is the slope of the frequency sweep also illustrated in figure A.1. The phase of the waveform can then be found by integrating the frequency from 0 to time t.

$$\phi(t) = 2\pi \int_0^t f(t)dt = 2\pi(f_c + \frac{1}{2}\alpha t)t \tag{A.2}$$

Given a transmit power A_t the transmitted signal s_t can be described as.

$$s_t(t) = A_t \cos[\phi_r] = A_t \cos[2\pi(f_c + \frac{1}{2}\alpha t)t] \tag{A.3}$$

In figure A.2 an illustration of the principles behind a FMCW radar can be seen.

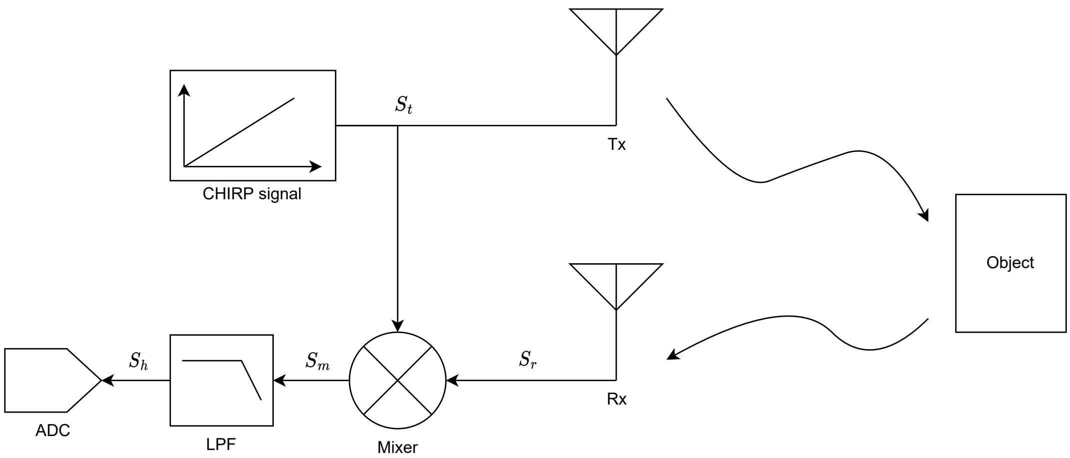

Figure A.2: Illustration of FMCW radar principle

Assuming that the transmitted signal s_t gets reflected from an object giving a τ time delay of the transmitted signal at the receiver (Rx).

$$s_r(t) = s_t(t-\tau) = A_r \cos[\phi_t(t)] = A_r \cos[2\pi((f_c + \frac{1}{2}\alpha(t-\tau))(t-\tau))] \tag{A.4}$$

$$= A_r \cos[2\pi(f_c(t-\tau) + \frac{1}{2}\alpha(t-\tau)^2)] \tag{A.5}$$

Where A_r is the received signal strength, The received signal is then down mixed with the transmitted signal s_t, giving:

$$s_m(t) = s_r(t)s_t(t) \tag{A.6}$$

$$= A_r A_t \cos[\phi_r(t)] \cos[\phi_t(t)] \tag{A.7}$$

Using the cosine product rule gives the following signal.

$$s_m(t) = A_r A_t \frac{cos[\phi_r(t) - \phi_t(t)] + cos[\phi_r(t) + \phi_t(t)]}{2} \tag{A.8}$$

From figure A.2 we see that a low pass filter (LPF) directly follows the mixer. The LPF removes the high frequency image $cos[\phi_r(t) + \phi_t(t)]$ from the mixing, the signal $s_h(t)$ to be sampled by the analog to digital converter (ADC) written as.

$$s_h(t) = A_r A_t \frac{1}{2} cos[\phi_r(t) - \phi_t(t)] \tag{A.9}$$

$$= A_r A_t \frac{1}{2} cos[2\pi(f_c(t-\tau) + \frac{1}{2}\alpha(t-\tau)^2) - (2\pi(f_c t + \frac{1}{2}\alpha t^2))] \tag{A.10}$$

$$= A_r A_t \frac{1}{2} cos[2\pi(f_c t - f_c\tau + \frac{1}{2}\alpha t^2 + \frac{1}{2}\alpha\tau^2 - \alpha t\tau - f_c t - \frac{1}{2}\alpha t^2)] \tag{A.11}$$

$$= A_r A_t \frac{1}{2} cos[2\pi(-f_c\tau - \alpha\tau t + \frac{1}{2}\alpha\tau^2] \tag{A.12}$$

The delay τ is time dependent when the target is moving with a velocity v_{obj} in respect to the radar. Assuming that the chirp period is much faster than a change in velocity for the target, the time dependent delay can be written as [2].

$$\tau = \frac{2(R + v_{obj}t)}{c} \tag{A.13}$$

Where R is the distance to the object, and c is the speed of light. Inserting equation (A.13) into equation (A.12) results in

$$s_h(t) = A_h \cos\left[2\pi\left(f_c \frac{2(R+v_{obj}t)}{c} - t\alpha\frac{2(R+v_{obj}t)}{c} + \frac{1}{2}\alpha\left(\frac{2(R+v_{obj}t)}{c}\right)^2\right)\right] \tag{A.14}$$

$$= A_h \cos[2\pi(f_c\frac{2R}{c} + tf_c\frac{2v_{obj}}{c} - t\alpha\frac{2R}{c} - t^2\alpha\frac{2v_{obj}}{c} \tag{A.15}$$

$$+ \frac{1}{2}\alpha\left(\frac{2R}{c}\right)^2 + \frac{1}{2}\alpha\left(\frac{2v_{obj}t}{c}\right)^2 + \frac{1}{2}\alpha 2t\frac{2R\cdot 2v_{obj}}{c})] \tag{A.16}$$

Letting the time difference from the distance be $\frac{2R}{c} = t_d$ and the doppler shift be $f_d = f_c\frac{2v_{obj}}{c}$ the equation can be rewritten

$$s_h(t) = A_h \cos\left[2\pi\left(f_c t_d + tf_d - t\alpha t_d - t^2\alpha\frac{2v_{obj}}{c} + \frac{1}{2}\alpha t_d^2 + \frac{1}{2}\alpha t^2\left(\frac{2v_{obj}}{c}\right)^2 + t\alpha t_d\frac{2v_{obj}}{c}\right)\right] \tag{A.17}$$

$$= A_h \cos\left[2\pi\left(f_c t_d - t\alpha t_d + t_d^2\alpha + tf_d + t^2\alpha\left(\frac{1}{2}\left(\frac{2v_{obj}}{c}\right)^2 - \frac{2v_{obj}}{c}\right) + t\alpha t_d\frac{2v_{obj}}{c}\right)\right] \tag{A.18}$$

Typically the term $t^2\alpha\left(\frac{1}{2}\left(\frac{2v_{obj}}{c}\right)^2 - \frac{2v_{obj}}{c}\right)$ is called the range doppler coupling.

The terms $t^2\alpha\left(\frac{1}{2}\left(\frac{2v_{obj}}{c}\right)^2 - \frac{2v_{obj}}{c}\right)$, $t\alpha t_d\frac{2v_{obj}}{c}$ and $t_d^2\alpha$ is neglected in most literature, due to the terms tend to be close to zero from the typically assumed radar waveform parameter (slope, BW and CHIRP Period *Tc*) [1]–[5]. Hence the signal can be reduced to the more simple form.

$$A_h \cos\left[2\pi\left(f_c t_d - t\alpha t_d + t_d^2\alpha + tf_d\right)\right] \tag{A.19}$$

The term $t\alpha t_d$ will give a certain frequency called the beat frequency $f_{beat} = \alpha t_d$ [1], [3].

A.2 Complex Baseband

A complex mixer can be used to down convert the signal, instead of a real mixer. Here the received signal is mixed down by the transmitted signal and a 90° phase shifted version giving the inphase s_I and quadrature signal s_Q. In figure A.3 a principle diagram can be seen.

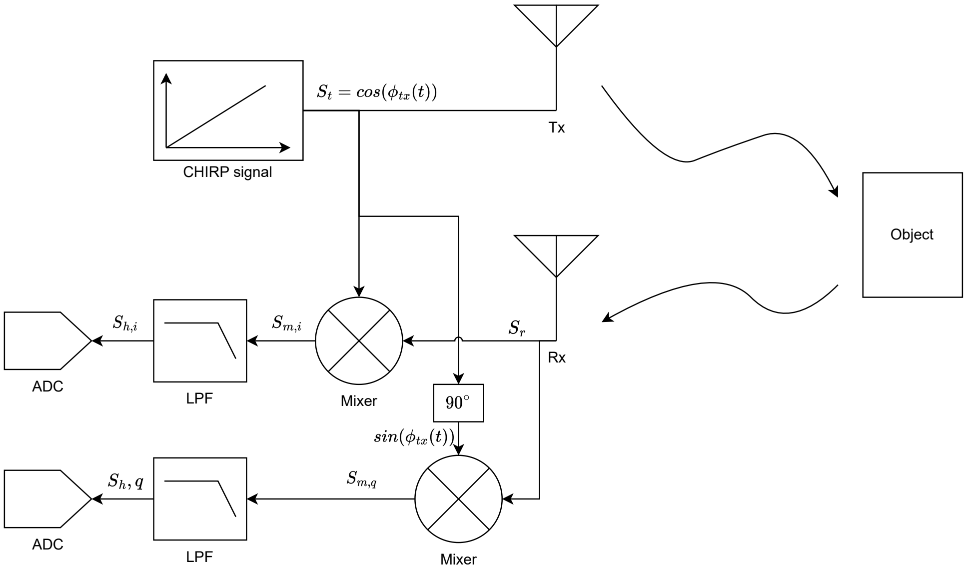

Figure A.3: Complex down conversion

The inphase signal s_I follows the resulting signal from equation (A.12). For the quadrature signal s_Q the following trigonmetric relation is used

$$\cos(\phi_r(t))\sin(\phi_t(t)) = \frac{\sin(\phi_r(t) + \phi_t(t)) - \sin(\phi_r(t) - \phi_t(t))}{2} \tag{A.20}$$

Since a LPF follows the quadrature mixing the $sin(\phi_r(t) + \phi_t(t))$ is removed. The resulting signal have the same phase as in equation (A.12), resulting in the in-phase and quadrature signal after LPF.

$$s_I(t) = A_r A_t \frac{1}{2}\cos[2\pi(f_c\tau - \alpha\tau t + \alpha\tau^2] \tag{A.21}$$

$$s_Q(t) = -A_r A_t \frac{1}{2}\sin[2\pi(f_c\tau - \alpha\tau t + \alpha\tau^2] \tag{A.22}$$

Adding the signal with s_Q being imaginary, results in the complex representation following Euler's identity $\exp(-j\theta) = cos(\theta) - jsin(\theta)$, with j being the imaginary unit.

$$s_c(t) = s_I(t) + js_Q(t) \tag{A.23}$$

$$= A_r A_t \frac{1}{2}\exp(-j2\pi(f_c\tau - \alpha\tau t + \alpha\tau^2) \tag{A.24}$$

Following the same expansion as previously, the same resulting phase from equation (A.18) can be represented in the complex representation.

$$s_{h,c}(t) = A_h \exp\left[-j2\pi\left(f_c t_d - t\alpha t_d + t_d^2\alpha + tf_d + t^2\alpha\left(\left(\frac{2v_{obj}}{c}\right)^2 - \frac{2v_{obj}}{c}\right) + t2\alpha t_d\frac{2v_{obj}}{c}\right)\right] \tag{A.25}$$

And the reduced form with the neglected terms removed.

$$s_{h,c}(t) = A_h \exp\left[-j2\pi\left(f_c t_d - t\alpha t_d + t_d^2\alpha + tf_d\right)\right] \tag{A.26}$$

A.3 MIMO Radar - Angle Estimation

A typical FMCW radar for automotive will have a antenna array at the receiver as illustrated in figure A.4. Assuming that the incident wave front is a plane wave, and that the antenna array have equal distance, there will be a constant phase shift between each antenna.

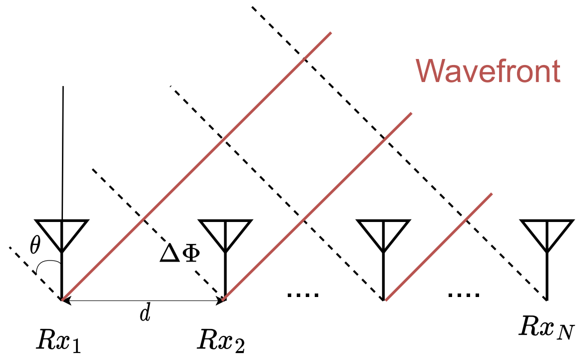

Figure A.4: Caption

For an incident plane wave arriving at an angle θ, at an antenna array with distance d between the antenna, the extra travel of the wave will be.

$$l = \sin(\theta)d \tag{A.27}$$

with a wavelength λ_c, the phase shift between two array elements is given by

$$\Delta\Phi = 2\pi\frac{l}{\lambda_c} = \frac{2\pi}{\lambda_c}\sin(\theta)d \tag{A.28}$$

The highest unambiguous phase shift is obtained with a distance $d = \frac{\lambda_c}{2}$, giving the maximum field of view.

$$\Delta\Phi = \frac{2\pi}{\lambda_c}\frac{\lambda_c}{2}\sin(\theta) = \pi sin(\theta) \tag{A.29}$$

The phase shift from the first antenna to the nth antenna will just be n times the phase shift between the first two.

$$\Delta\Phi_{1,n} = n\pi\sin(\theta) \tag{A.30}$$

The number of Rx antennas sets the resolution of the estimated angle of arrival (AoA). An increase in Rx ports will increase the cost and complexity of the system, therefor, virtual antenna array. With virtual antenna array multiple Tx ports are used, to virtually increase the Rx antenna array. The principle can be seen in figure A.5 [6].

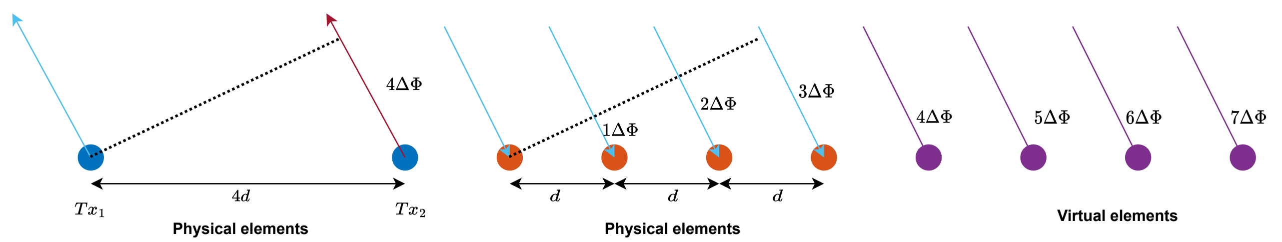

Figure A.5: Illustration of virtual antenna array for extending the amount of Rx elements for AoA estimation, the figure is inspired from [6].

By having the second Tx_2 antenna placed exactly Nd apart from the first Tx_1, will give a phase shift equal to $N\Delta\Phi$ with N being the number of Rx antenna. The signal at the Rx antenna will therefore give new shifted virtual elements, corresponding to the shift between the Tx antennas.

Beside extending the resolution in one angle, the same methodology can be used to extend the array so both elevation and azimuth can be estimated. The second Tx must then be placed vertically shifted as illustrated in figure A.6.

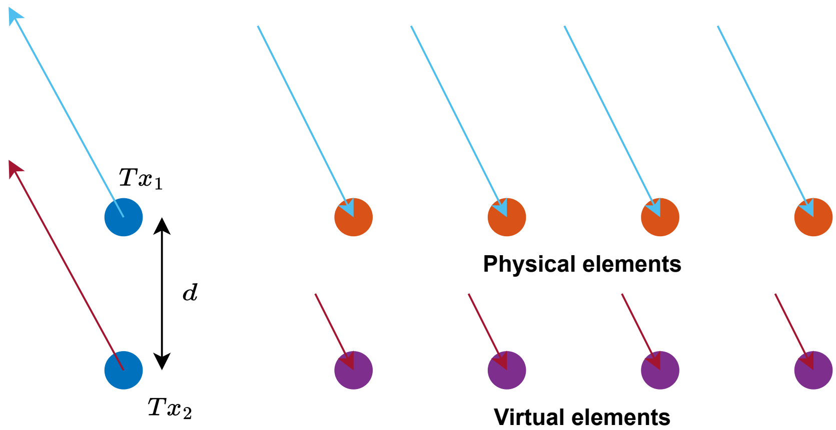

Figure A.6: Illustration of virtual antenna array, with extension in the vertical axis making a 2D array, illustration is inspired from [6].

To use virtual antenna array the signal (CHIRP) is first transmitted at oneTx antenna and afterwards on the other. The measurement time will therefore double with the use of two Tx antenna. For the received signal equation to be valid the distance and velocity must be assumed constant doing the CHIRP time at both Tx antennas. Increasing the angle resolution with virtual elements is therefore a compromise with the CHIRP period T_c.

A.4 Ti IWR1443 Evaluation Board

Texas Instruments (TI) have developed a range of mmWave radar IC. They divide them into two categories, industrial and automotive. Furthermore, the amount of integration varies between the different chips, having varying capabilities in terms of on chip processing capabilities. Doing the project an IWR1443 chip was available, being integrated into a development board.

The IWR1443 is an industrial application IC mmWave radar working in the frequency bands from 78-61 GHz. In figure A.7 a principle diagram of the chip is seen. The chip allows have 4 Rx ports and 3 Tx ports. A diagram of the chip can be seen in figure A.7.

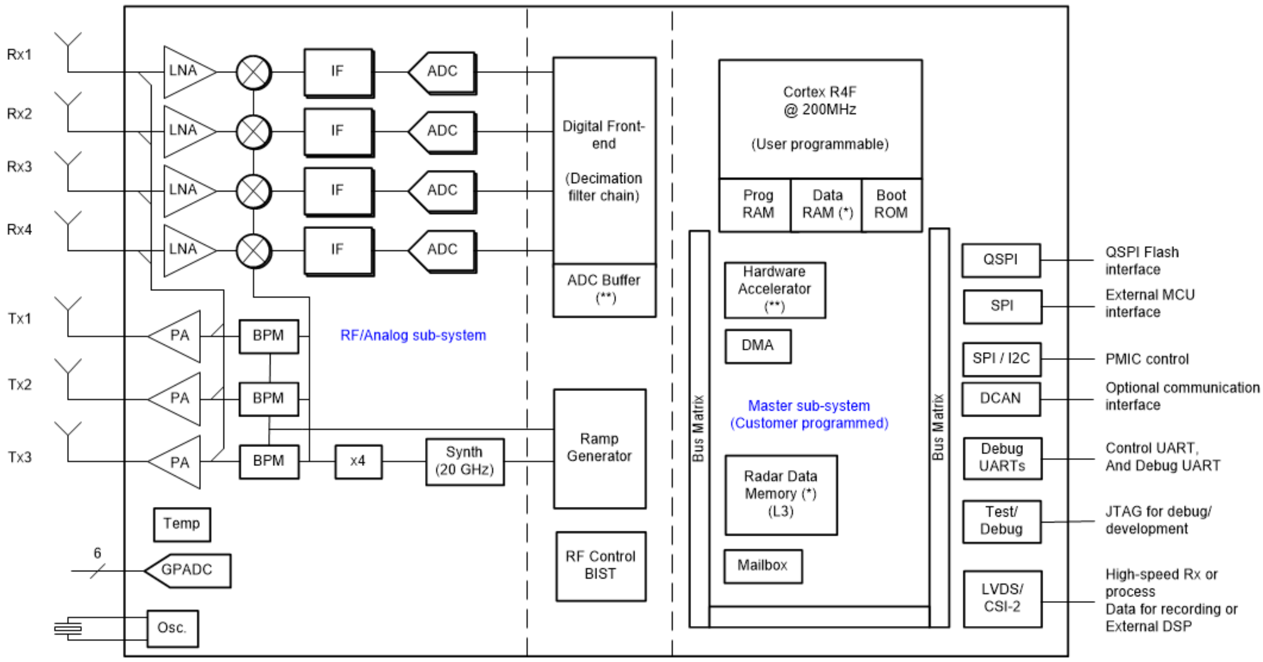

Figure A.7: Diagram of IWR1443, picture from [7]

For demonstration purposes TI have made a demonstration board, with a uniform linear array (ULA) patch antennas, as seen in figure A.8. Each antenna port goes to an antenna array with three patch antennas. The antenna array at each port is for narrowing the beam-width in the elevation angle [8].

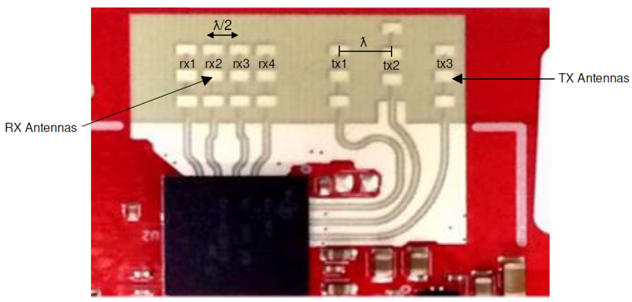

Figure A.8: Picture of antenna part of IWR1443 Boost evaluation module. The picture is from [8]

The evaluation board, comes with pre made code for running on the IWR1443 chip, based on the manufactures recommendations. Typically the application is limited by the amount of available memory, since saving multiple Chirps with a certain sample density quickly takes up a significant amount of memory space. Furthermore, the amount of measurement points require a higher amount of calculations, therefore the application might be limited by the calculation speed. The general algorithm on the chip is seen in figure A.9.

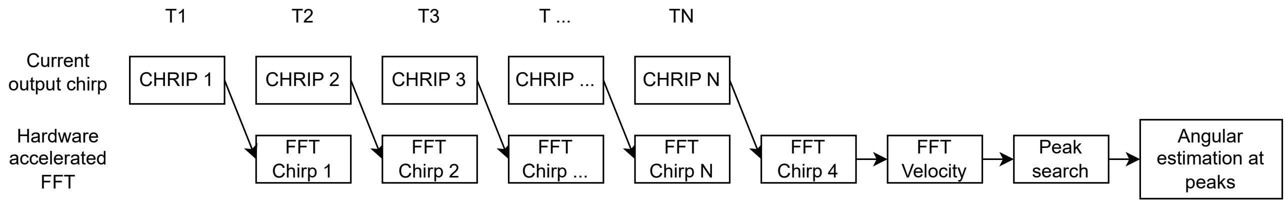

Figure A.9: Simplified diagram of the algorithm provided by TI for the evaluation board.

The properties of the radar under test (RuT) presented in the paper (Table III), is based on number for a TI automotive sensor AWR2943 [9]. Compared to the IWR1443, the chip have a higher memory capacity, and furthermore a higher amount of memory available. Hence the limitations witch was found by experimentation with the IWR1443 might not be as relevant. For the paper, both signal processing a memory was not taken into account and only the radar specification (BW, sample speed, IF frequency number of antenna ports etc.) was included. The radar performance in the simulation might therefore be higher than the capabilities of an actual chip.

Bibliography

[1] C. Lovescu and S. Rao, "The fundamentals of millimeter wave radar sensors," Texas Instruemnts, Tech. Rep., 2020.

[2] V. Winkler, "Range Doppler detection for automotive FMCW radars," in *2007 European Microwave Conference*, 2007, pp. 1445–1448. DOI: 10.1109/EUMC.2007.4405477.

[3] J.-J. Lin, Y.-P. Li, W.-C. Hsu, and T.-S. Lee, "Design of an FMCW radar baseband signal processing system for automotive application," *SpringerPlus*, vol. 5, Dec. 2016. DOI: 10.1186/s40064-015-1583-5.

[4] J.-P. Artis and S. Kemkemian, "The radar in the automotive domain," *SpringerPlus*, 2005. DOI: 10.1007/BF03219824.

[5] F. Rafieinia and K. Haghighi, "ASGARDI: A Novel Frequency-based Automotive Radar Target Simulator," in *2020 IEEE MTT-S International Conference on Microwaves for Intelligent Mobility (ICMIM)*, 2020, pp. 1–4. DOI: 10.1109/ICMIM48759.2020.9299008.

[6] S. Rao, "MIMO Radar," Texas Instruemnts, Tech. Rep., 2018.

[7] T. Instruments, *IWR1443, Single-chip 76-GHz to 81-GHz mmWave sensor integrating MCU and hardware accelerator*, https://www.ti.com/product/IWR1443, Accessed: 24-05-2023.

[8] *IWR1443BOOST Evaluation Module mmWave Sensing Solution*, SWRU518D, Texas Instruemnts, 2017.

[9] T. Instruments, *AWR2944 Automotive, second-generation 76-GHz to 81-GHz high-performance SoC for corner and long-range radar*, https://www.ti.com/product/AWR2944, Accessed: 24-05-2023.